Polymer Testing 128 (2023) 108217

Contents lists available at ScienceDirect

Polymer Testing

journal homepage: www.elsevier.com/locate/polytest

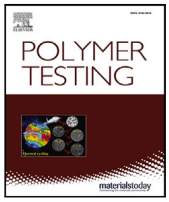

Investigation of the ductile deformation potential of microscale epoxy materials

Janina Mittelhaus *, Phil Röttger, Eduard Schill, Julius Jacobs, Bodo Fiedler

Hamburg University of Technology, Institute of Polymers and Composites, Denickestraße 15, 21073 Hamburg, Germany

ARTICLE INFO

Keywords:
Brittle-to-ductile transition
Plasticity
Thermomechanical behavior
Size effect
Infrared spectroscopy
Peak shift

ABSTRACT

In fiber reinforced polymers (FRP), the matrix, e.g. an epoxy system, usually has a microscopic size and therefore may have other properties than the standard bulk samples. It is known that a size effect exists, for epoxy also in terms of ductility or plasticity. However, to date, there is no physical, mechanochemical or molecular explanation for the correlation of plasticity and gauge volume, especially for an archetypical brittle standard epoxy matrix. The specific limits of the gauge volume for these ductile effects are unknown as well. Therefore, a new manufacturing method to produce thin epoxy films with thicknesses between 15 and 100 μm is developed. These films are investigated by differential scanning calorimetry (DSC) with regard to the degree of cross-linking. The mechanical properties are determined by tensile and creep test, also at different temperatures. In the next step, a suitable analysis method for the correlation of molecular structure and mechanical deformation behavior is developed. Manufactured films are investigated by *ex situ* and *in situ* infrared spectroscopy (IR) to analyze the molecular mechanisms caused by load introduction. Various pre-processing and interpretation methods for the determination of spectral changes, such as peak shifts, are used to figure out the specific molecular changes related to the mechanical stress from the raw spectral data. It was possible to detect molecular changes of the highly cross-linked macromolecules as a result of plastic deformation caused by tensile load. Shear bands and necking are visualized by photoelastic analysis and a better understanding of the brittle material's ability to form shear bands is achieved.

1. Introduction

FRPs are widely used for high-quality applications that require excellent (anisotropic) mechanical properties combined with low weight, e.g. in the sectors of aerospace, wind energy and automotive. The structure of FRP consists of oriented fibers surrounded by a matrix material, such as an epoxy resin system. This results in zones of interconnected matrix materials that are in the (sub-) micrometer range, such as resin-rich zones between fibers (1–25 μm, intralayer) and between reinforcing prepregs or layers (10–200 μm, interlayer) [1]. However, characterization of matrix materials such as epoxy is generally performed on a macroscopic bulk scale following standardized test methods such as ASTM D638 [2] or DIN EN ISO 527 [3]. By using mechanical bulk parameters as input for microscale modeling of composites [1,4–10], an insufficient agreement between the modeled and observed properties can occur [11]. One reason is the deviation of the mechanical behavior of the microscopic matrix from the macroscopic standard bulk samples [1]. Therefore, a detailed insight into the micromechanical properties and deformation behavior of the thermoset matrix as a microcomponent of composites is significant for the improvement and optimization of polymeric composites.

The mechanical properties of a material are a manifestation of the way in which individual bonds within the materials respond to the applied macroscopic stress [12]. Fourier transform infrared (IR) spectroscopy can be used to study the deformation mechanisms of materials on a microstructural level due to mechanical loading and to gain insight into the molecular causes of their mechanical properties [13,14]. It was found that during mechanically induced stretching of the carbon skeleton in molecules, the associated vibration frequency corresponding to the maximum of certain infrared peaks decreases [15–20]. This behavior is explained by changes in the molecular structure such as variations in the force constants k, bond lengths l, valence angles and the internal rotation angles [21]. This approach is often used when studying composite materials [4,5,10,22–26]. This indirect measurement method has also been applied, for example, to aramid, carbon, poly(p-phenylene-2,6-benzobisoxazole) (PBO) and polyethylene terephthalate (PET) fibers [27–33] or to biomaterials such as cellulose [34–38], silkworms [39] and spider silk [40]. To apply this

* Corresponding author.
E-mail address: janina.mittelhaus@tuhh.de (J. Mittelhaus).

https://doi.org/10.1016/j.polymertesting.2023.108217
Received 21 June 2023; Received in revised form 1 September 2023; Accepted 18 September 2023
Available online 23 September 2023

method as well to the complex 3D cross-linked thermoset and to get a deeper insight for epoxy, suitable microscale samples are first required. In some studies, epoxy resin systems in the form of microscale fibers are selected for micromechanical analysis. However, because of the curved surface of these fibers, they are not suitable for transmission infrared (IR) spectroscopy investigations. Therefore, a new manufacturing process for epoxy films with different, adjustable and reproducible thicknesses is developed as well as an adapted *in situ* IR analytic. Care was taken with the film thicknesses selected to ensure that they are sufficiently thin to avoid total absorbance in IR transmission measurements. Only with sufficient IR transmittance, it is possible to determine all spectral information.

2. Materials and methods

A low viscosity resin system consisting of EPIKOTE™ Resin MGS RIMR 135, which is based on diglycidyl ether of bisphenol A (DGEBA), combined with a liquid aliphatic diamine hardener, EPIKOTE™ Curing Agent MGS RIMH 137 (Hexion, International: USA/Europe) is used. Both components are mixed in a weight ratio of 100:30 in a mixer (SpeedMixer DAC 150.1 FVZ) at 3500 rpm for 5 min. The backbone of the DGEBA also contains aromatic rings, or more precisely the para-phenylene group, which is a decisive factor in the following study.

2.1. Epoxy film manufacturing

A new infusion manufacturing process was developed to produce thermoset films from the resin system presented. For this purpose, two glass plates with identical dimensions of 250 mm × 250 mm are placed on top of each other. A seal is placed between these glass plates, thus creating an infusion chamber. To obtain a resulting film thickness of 15 μm, 30 μm, 50 μm and 100 μm, feeler gauges with defined and appropriate thicknesses depending on the target film thickness and double-sided 5 μm thick transfer adhesive tape (Supplier FFT Group) are used. Therefore, the transfer adhesive tape is placed on both sides of the chosen feeler gauge. Two frames of 80 mm × 40 mm are created side by side with the 'seal system'. Since the films cannot be removed from the glass plates without causing defects and a release agent should not be used (risk of influencing the cross-linking reaction), a suitable carrier film is required. In the course of preliminary tests, a series of substrate materials were extensively analyzed with regard to wetting behavior and release properties. A low density polyethylene (LDPE) film (DM Folien GmbH) met the requirement profile and is therefore positioned between the glass plates and the 'seal'. The setup is shown in Fig. 1. In the next step, the entire set-up is placed between two metal plates (including rubber protection) with several screws. They are used to tighten the seal across the entire surface so that the gap is maintained and no resin escapes through the seal. In the last step, the entire construction is positioned upright, and the liquid resin is gradually filled into the gap between the two glass plates using a syringe. After approximately 2 h, the cavity is completely filled with the liquid resin due to the acting gravitational and capillary forces. Subsequently, the curing takes place inside the cavity or glass plates at room temperature for 72 h. During demolding, care was taken to avoid introducing additional, extensive stresses and strains into the epoxy films. After demolding, the cured epoxy films are post-cured at 80 °C for 15 h in a convection oven. For the post-curing process, the films are clamped in a metallic frame to prevent the films from curling. Care is taken to ensure that the films are not stretched during this process. Subsequently, the films are conditioned at 23 ± 2 °C and 30 ± 10% relative humidity for at least 96 h.

With this manufacturing procedure, films with thicknesses close to the chosen target thickness are available. The specimens are then punched out and film specimens with a thickness of 14.36 ± 3.35 μm, 32.36 ± 2.0 μm, 50.94 ± 1.02 μm and 102.11 ± 3.16 μm are obtained. A dial gauge is used to determine the thicknesses at seven different specimen positions in the gauge length. The utilized dogbone geometry can be seen in Fig. 2. The geometric dimensions deviate from the established standard DIN EN ISO 527-3, as they are predefined by the Deben microtest stage used which is located in the IR sample cabinet for *in situ* IR measurements during mechanical loading.

In addition to epoxy films, bulk standard epoxy plates with a thickness of 2 mm are produced with a Resin Transfer Molding (RTM) process as a reference. The RTM process is followed by a curing and post-curing process identical to that of the films (72 h@RT and 15 h@80 °C). Subsequently, the plates are conditioned at 23 ± 2 °C and 30 ± 10% relative humidity for at least 96 h.

2.2. Characterization of epoxy films

In order to exclude possible large or measurable defects caused by the demolding or punching process, microscope images are taken after machining using a Keyence digital microscope (VHX-6000). The possibility of whether components of the LDPE carrier film diffuse into the epoxy films or whether the hardener diffuses away into the LDPE film during manufacturing or the cross-linking reaction is to be ruled out. For this purpose, surface-sensitive IR total reflectance (ATR) measurements are carried out on the manufactured epoxy films and the LDPE carrier films additionally as a method of analyzing the chemical structure of surface areas. No measurable chemical changes were detected in any of the investigated films. Moreover, the spectra of epoxy films (transmission IR) are compared with spectra of the RTM bulk plate (ATR).

For further characterization of the film specimens, temperature-modulated differential scanning calorimetry (TM-DSC) measurements are performed with a DSC 204 F1 (Netzsch). The samples are cut from the manufactured epoxy films using a circular punch with a slightly smaller diameter than the crucibles used. The generated epoxy film sheets are then stacked flat on top of each other in the crucible. The number of film sheets is selected according to the target weight of 9–11 mg and therefore depends on the thickness chosen for the film. In total, at least three different epoxy films per thickness are analyzed with DSC. To rule out a possible significant difference between films and bulk samples in terms of cross-linking behavior or glass transition temperature (T_g), the T_g of three bulk samples from the 2 mm thick RTM plates are also investigated. To exclude any possible influence of the sample shape on DSC measurement, bulk cuts or sheets are also created from a cast rod sample (diameter: 10 mm, height: 50 mm, similar curing profile as films and RTM plates) with a rotation microtome (Thermo Scientific Microm HM 340 E, thickness approximately 70 μm). These sheets are also positioned on top of each other in the crucible in a way analogous to that of the punched-out film sheets. In summary, there are three different sample configurations for the DSC measurements: 1. films with different thicknesses 2. bulk samples from the RTM plates 3. Microtome cuts from a bulk samples. For the determination of the glass transition temperature, a linear heating of 2 K/min from 20 °C to 150 °C is applied to all samples. Modulation is carried out with a period of 60 s and an amplitude of 1 K. According to DIN EN ISO 11357-2, the glass transition temperature can be identified by the inflection point method [41]. In this case, the glass transition temperature is determined using the maximum negative slope via the first derivative of the first heating curve in a specified interval. In addition, the first heating curve is checked with regard to exothermic reactions, in order to obtain information about any unreacted resin and hardener components that may remain after the post-curing process, since the surface area of the films is very large compared to its volume. This can promote evaporation of the hardener, which in itself results in a non-stoichiometric ratio of resin and hardener and thus incomplete cross-linking.

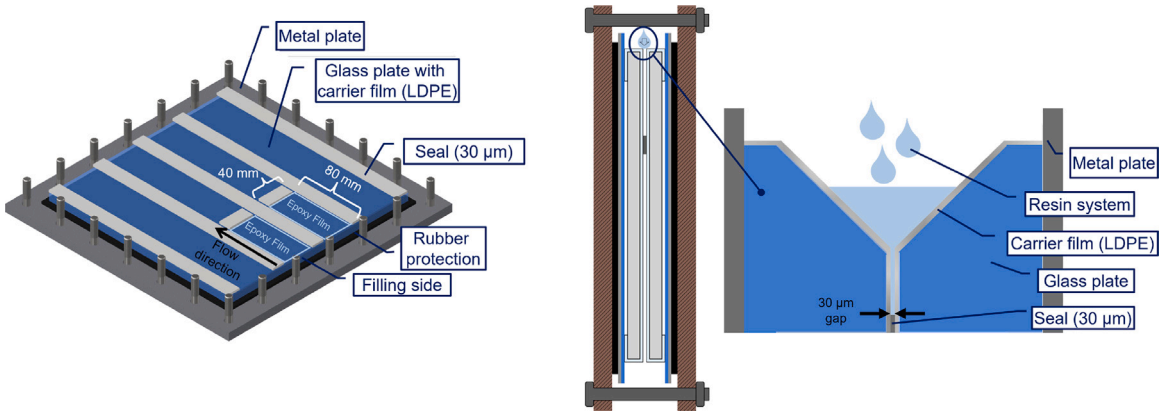

Fig. 1. Schematic setup for manufacturing process of epoxy films in top view (left) and side view (middle and right), here with a target film thickness of 30 µm.

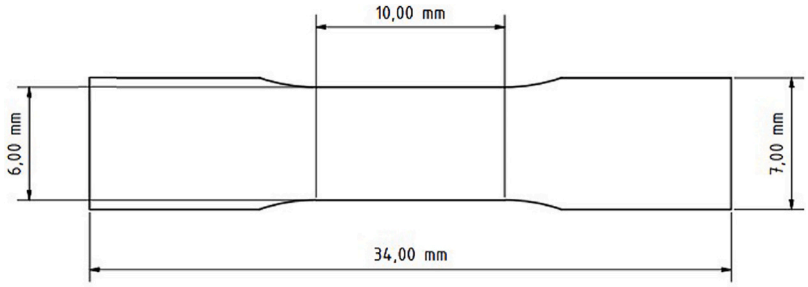

Fig. 2. Geometry of dogbone specimen resulting from punching process of the films. The sample geometry is used for all mechanical tests.

2.3. Mechanical testing

The manufactured thin epoxy films are mechanically tested and investigated with *ex situ* and *in situ* infrared spectroscopy (IR) to identify geometric changes in load-bearing molecules that result in a so-called peak shift and other spectral changes.

2.3.1. Tensile tests at room temperature

Previous to mechanical testing, all film samples are analyzed by IR (see 2.4.1). The mechanical properties of the film specimens are then determined by tensile tests according to DIN EN ISO 527-3. A Zwick Roell Z2.5 tensile machine is used for these tests at room temperature. Preliminary tests showed that the films frequently failed in the clamping jaw area, probably due to damage of the specimen caused by contact pressure or the clamping jaw surface. Furthermore, it is difficult to clamp and align thin film specimens between the clamping jaws. For this reason, a suitable paper frame is used to fix the film specimens analogue to ASTM D3379 for single-fiber tensile tests. The schematic setup is shown in Fig. 4 (right). The samples (glued onto the paper frame) are clamped in the jaws and care is taken to ensure that the specimen is clamped vertically and without applying tension. After clamping, the two paper bars of the paper frame are cut. The gauge length of the samples is 10 mm (see Fig. 2). The samples are loaded at a constant strain rate of 1 mm/min. The change in length or strain is recorded via a video extensometer. The testXpert-II program and a load cell 50 N are used. After mechanical testing and failure, representative specimens are analyzed again by IR (see 2.4.1).

To obtain information about the local strain distribution during the tensile test, digital image correlation (DIC) measurements are carried out using the Aramis software. For this purpose, white and black paint is applied to some additional film samples in a speckled pattern after the samples were placed and glued onto the paper frame. In order to exclude an influence of the DIC paint on the mechanical parameters, films with DIC paint are not taken into account in the determination of the mechanical parameters.

As a reference, six standard bulk samples of the RTM plates (specimen type 1BA according to DIN EN ISO 527-2) are additionally tensile tested. These tests are performed with a Zwick Z010 tensile machine and a 10 kN load cell with constant strain rate of 1 mm/min at room temperature. The strain is determined via the crosshead displacement. This allows comparison of bulk and films, i.e. the influence of the test volume on the mechanical behavior. The bulk epoxy sample type 1AB has a test volume of approximately 250 mm^3 and the epoxy films with a thickness of 30 µm generated a gauge volume of approximately 1.8 mm^3 (see Fig. 2). That is about a factor of approximately 140 times less than the test volume of standard bulk samples.

2.3.2. Tensile tests at different temperatures

In addition, films specimens with a thickness of 50 µm are subjected to tensile tests at temperatures that deviate from room temperature to analyze the influence of the test temperature on the ductility and molecular processes that occur during plastic deformation also. The test temperatures are set to T = 3, 13, 33, 43, 53 °C, respectively. Before mechanical testing, the specimens are analyzed by IR (see 2.4.1). Tensile tests are performed on a Dynamic Mechanical Thermal Analysis (DMTA) test machine of the Gabo Eplexor 500 N type with a constant strain rate of 1 mm/min. During the mechanical test, the specimen is placed in a climatic chamber with a defined and controlled test temperature. Here, the specimen is clamped without a paper frame, but with gripping tabs in the clamping area made of crepe tape. Five specimens with a gauge length of 10 mm (see Fig. 2) are tested for each temperature. The strain is determined by the displacement of the crosshead. After mechanical testing and failure, some specimens are analyzed again by IR (see 2.4.1).

2.3.3. Creep tests at room temperature

The creep tests are carried out with a Deben tensile microstage with a 20 N load cell at room temperature on film specimens according to EN ISO 899-1 to analyze the impact of time on the microstructural changes under mechanical stress. This device can be installed in the IR sample

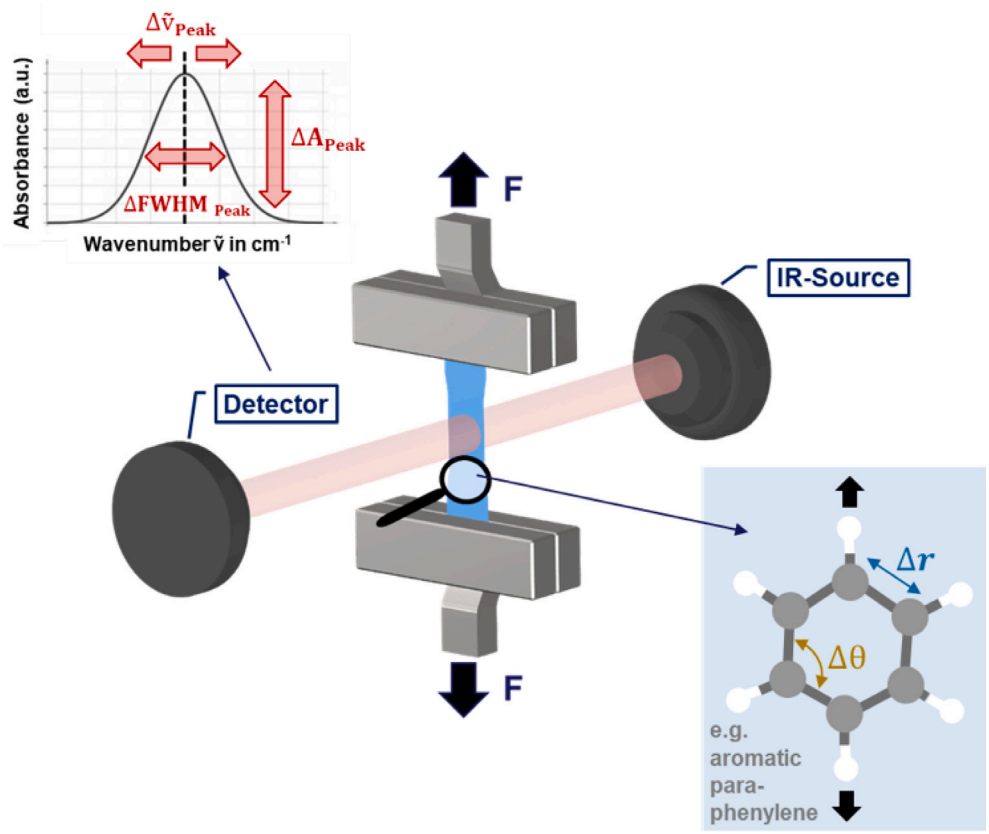

Fig. 3. Schematic overview of in-situ setup (mechanical testing + IR). The molecular structure (bond length r and bond angles θ) changes due to mechanical load introduction and thus causes changes in the IR spectra. Resulting changes could be peak shifts ($\Delta\tilde{\nu}_{Peak}$), a change in the peak width ($\Delta FWHM_{Peak}$) and a variance in the peak absorbance (ΔA_{Peak}).

chamber together with an already clamped film sample. The Deben stage is controlled by the corresponding Deben software V 6.10. The creep tests are performed at a stress level of approximately 56 MPa. This corresponds to approximately 80% of the Ultimate Tensile Strength (UTS) of the tensile test performed with the Zwick Roell Z2.5 epoxy films with a thickness of 30 µm at room temperature (see 2.3.1 and 3.2.1). Stress is generated at a strain rate of 1 mm/min at the beginning of the test. The gauge length of the specimens is also 10 mm (see Fig. 2).

2.4. Infrared spectroscopy

All the IR measurements are performed with a Bruker TENSOR II instrument. The OPUS 7.5 software is provided to adjust the settings for the measurements. The resolution is 2 cm^{-1}, the aperture is set to 5 mm and data from the mid-infrared (MIR) range of 4800 cm^{-1} to 500 cm^{-1} in transmission mode are recorded. For all measurements performed, 40 background spectra are taken from the atmospheric environment in the sample chamber without a specimen before starting the experiment.

2.4.1. Ex siu infrared spectroscopy

Using the IR standard method, the specimen is not examined during load, but before and after the mechanical test, it is a so-called *ex situ* measurement. Thereby, eight sample spectra are recorded per specimen position, and from this an averaged spectrum for the specific sample position is generated by OPUS. This is done for the tensile tested specimens at room temperature (see 2.3.1) and at other temperatures (see 2.3.2).

2.4.2. In situ infrared spectroscopy

Using the *in situ* IR method, spectra are recorded during mechanical creep loading. The schematic setup is shown in Fig. 3.

In this study, *in situ* IR measurements are performed only at creep load to generate a longer IR measurement time due to the longer duration of mechanical load compared to a tensile test and to investigate time-related plastic effects. For this purpose, a single spectrum is recorded every 7 s at a defined and fixed position of the sample. This allows the wavenumber of selected bonds or vibrational modes to be tracked over time or during mechanical creep testing. For *in situ* IR mechanical tests, the Deben tensile microstage presented in the previous Section 2.3.3 is used and inserted into the Tensor II sample chamber. Due to the high absorbance of the IR radiation from the thicker films (50 µm and 100 µm) and the rather challenging handling of the 15 µm samples, in this *in situ* study IR spectra are only recorded for the 30 µm film samples during the creep test.

2.5. Photoelasticity

In addition to mechanical tests and IR investigations, photoelasticity is used as a further supplementary method. With the use of polarized light, the stress distribution in the translucent and loaded epoxy films can be studied. For this purpose, a Keyence VHX-6000 microscope is used together with a VH-Z20 and VH-ZST polarization adapter after mechanical loading. The measurement is performed in transmitted light mode, i.e. the translucent epoxy film is positioned on a glass specimen holder.

3. Results and discussion

3.1. Characterization of epoxy films

Comparing the processed spectra of epoxy films (transmission IR) and the spectra (processed in the same way) of the RTM bulk plate

(ATR), no significant spectral variations, which would indicate differences in the chemical structure, were observed. These results confirm that there are no microstructural differences between the epoxy films and bulk specimens visible with IR or ATR.

For the DSC measurement in total three different epoxy films per thickness are investigated. The glass transition temperature (T_g) determined from the first heating curve (thermal mechanical material history) of the DSC measurement after the post-curing process for all epoxy films is 89.0 ± 3.1 °C. The T_g of three samples taken from RTM plates is 87.1 ± 0.7 °C. The bulk microtome slice or cuts of three different bulk samples have a T_g of 88.0 ± 0.9 °C. An exothermic reaction in the first heating cycle is excluded for all DSC samples. All T_g values correspond to the Hexion data sheet (T_g around 90 °C), so that an intended degree of cross-linking can be assumed for bulk samples as well as for the films with different thicknesses. There is no indication of incomplete cross-linking caused, for example, by hardener evaporation due to the large surface of the films compared to volume, which was found for epoxy microdroplets [42].

3.2. Mechanical testing

3.2.1. Tensile tests at room temperature

At least ten film specimens for each sample thickness are subjected to tensile tests at room temperature with a strain rate of 1 mm/min and compared with the bulk properties. Five samples are examined perpendicular to the flow direction of the epoxy during the manufacturing process and five in the production direction according to DIN EN 527-3. The elongation at break and tensile strength is slightly higher for the specimen that are punched out in the epoxy flow direction. To exclude molecular orientation or anisotropy due to manufacturing as a reason for this behavior, polarized IR measurements with a Bruker Tensor II and a polarizer made out of BaF_2 were performed. The absorbance has the same intensity for all polarization directions, so no significant molecular anisotropy as a consequence of the resin flow direction is detectable. The cause of the slightly different mechanical properties of both types of film specimens may be due to the extrusion grooves of the LDPE carrier films, which are to some extent transferred to the epoxy films in the flow direction due to the applied pressure of the screws and the flow behavior during the manufacturing process (see 2.1). This was also verified by an investigation of as-produced epoxy film samples with a digital microscope.

The Young's modulus of the film specimen tested with a thickness of 30 µm in the epoxy flow direction is 3043 ± 170 MPa, the tensile strength can be reported as 69.8 ± 1 MPa and the elongation at break is 7.5 ± 2.9%. This corresponds to the mechanical results of samples of other thicknesses (see Table 1). All these values are within the range of the Hexion data sheet (σ = 60–75 MPa, E = 2700–3.200 MPa, ϵ = 5%–12%). The mechanical results also show that there is no measurable anisotropy in the specimens due to the manufacturing process, since the respective mechanical parameters along and across the epoxy flow direction do not differ significantly from each other. Even films with a greatly reduced thickness behave isotropically.

For each thickness a representative stress–strain curve in epoxy flow direction is shown in Fig. 4. In addition, a representative curve of a standard RTM bulk specimen is included as reference.

When comparing the curves and the mechanical properties (see Table 1), it is noticeable that the bulk specimens achieve higher strengths. This may be due to the film sample manufacturing process. The punched edges exhibit increased roughness, which under load leads to stress concentrations and failure at lower stresses. This effect is more severe for thinner films. This has also been previously described by other researchers [43,44] and is due to the fact that at these small scales, any defects in the specimens will have a greater influence on the mechanical properties (e.g., premature failure) than in specimens with bulk dimensions. The stiffness of the bulk specimens is slightly lower than the Young's modulus of the film samples. One reason for this may be the different strain measurement methods for the film and bulk specimens. The elongation at break of the bulk specimens tends to be lower than that of the film specimens. It is noticeable that the bulk and film curves differ significantly, since the film curves indicate a necking behavior and a steady-state plastic flow, which leads to a drop in the engineering stress. This was also obtained for microscale epoxy fibers, for example, in the study of Verschatse et al. [1], but not to a significant extent for bulk samples.

Table 1
Mechanical parameters (tensile strengths (σ), Young's modulus (E) and elongation at break (ϵ_b)) of the different epoxy specimens determined in a tensile test using a Zwick Z2.5 and Z 10.0 with a strain rate of 1 mm/min at room temperature.

	Film thickness in µm				Bulk
	15	30	50	100	
$\sigma_\parallel$ in MPa	63.1 ± 3.5	69.8 ± 1.0	71.2 ± 1.1	70.4 ± 0.4	78.9 ± 1.1
$\sigma_\perp$ in MPa	61.2 ± 6.2	68.8 ± 2.7	69.4 ± 0.7	69.5 ± 1.2	
$E_\parallel$ in MPa	2642 ± 201	3043 ± 170	3242 ± 133	3024 ± 122	2708 ± 33
$E_\perp$ in MPa	2646 ± 385	3153 ± 168	3135 ± 270	3032 ± 68	
$\epsilon_\parallel$ in %	8.0 ± 3.7	7.5 ± 2.9	11.5 ± 6.0	20.7 ± 8.0	8.4 ± 1.2
$\epsilon_\perp$ in %	6.1 ± 3.9	6.5 ± 3.6	6.7 ± 2.1	10.6 ± 4.9	

3.2.2. Tensile tests at different temperatures

According to DIN EN ISO 527-3, at least five film samples with a thickness of 50 µm per temperature are tested with the Gabor Eplexor DMTA test machine and a strain rate of 1 mm/min. In Fig. 5 representative stress–strain curves of three different temperatures are shown.

The pronounced plasticity of the film specimens is noticeable in these curves, too, even at lower temperatures (T = 3 °C). It can be seen that tensile tested specimens at higher temperatures (T = 43 °C) are associated with a lower tensile strength, a higher elongation at break and a lower Young's modulus. These mechanical behaviors at lower and higher temperatures as room temperature correspond to other studies on thermosets in general and on the same epoxy material in particular [45]. The main difference is that epoxy as film specimen shows plastic deformation in the form of pronounced shear bands, even at low temperature. *Ex situ* and *in situ* IR analysis can provide more information on the influence of temperature on changes in molecular structure induced by mechanical loading.

3.2.3. Creep tests at room temperature

The *in situ* IR creep test approach is expected to provide a deeper insight into the deformation process by acquiring time-dependent mechanical data. A total of twelve samples are examined with a thickness of 30 µm. Fig. 6 shows the creep curve of a representative sample with a thickness of 30 µm, which reaches the maximum strain of 16% that can be performed with the Deben tensile microstage without failure.

This graph represents the three phases of creep behavior. Within the first few seconds, spontaneous elastic and viscoelastic deformations cause the specimen to elongate during the initial loading and decrease in creep velocity due to hardening processes (creep phase 1). As time progresses, there is a constant and low creep rate and the beginning of a continuous reduction in the transverse section due to constant load application (creep phase 2). As a result, the true stress in the contracted test area is increased accordingly, whereas the nominal stress in the graph is constant. Finally, the creep strain increases until fracture occurs (excess stress due to local necking or irreversible material changes) (creep phase 3). The necking behavior observed here, however, is unusual for the typically more brittle epoxy resin.

3.3. Photoelasticity and DIC

Fig. 7 shows birefringence images of a representative creep-loaded film specimen with a thickness of 30 µm at an elongation of 16% (left). Additionally a representative specimen with a thickness of 30 µm

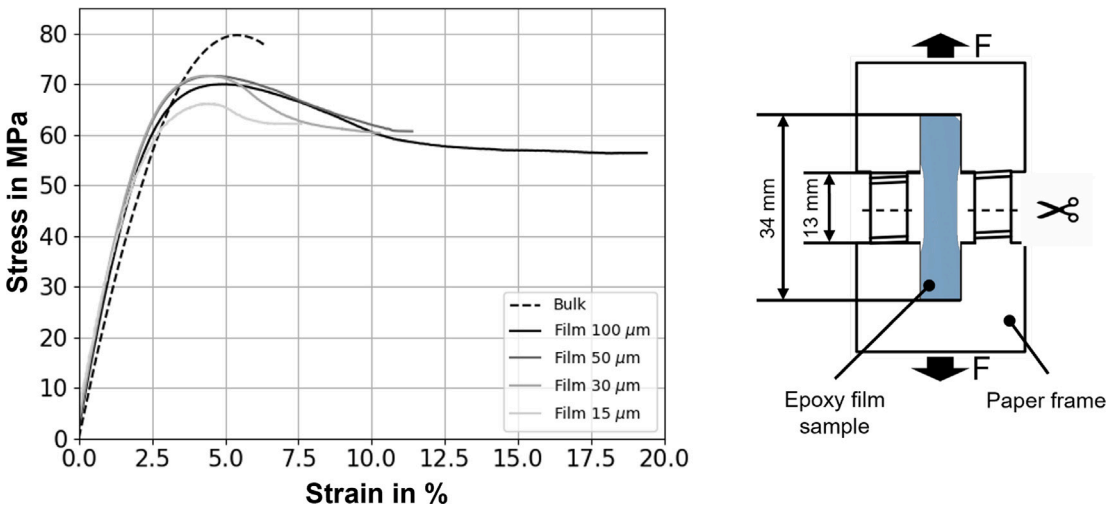

Fig. 4. Representative stress–strain curves of film samples with a thickness of 15, 30, 50 and 100 µm and a bulk reference, all loaded with a strain rate of 1 mm/min at room temperature (left). And the schematic setup for a loaded film specimen including the paper frame in top view (right).

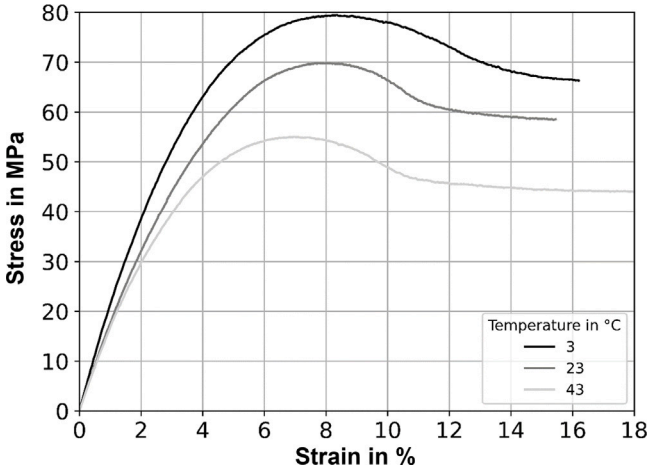

Fig. 5. Representative stress–strain curves for film samples with a thickness of 50 µm and a strain rate of 1 mm/min at different temperatures.

tensile-tested at room temperature, which reaches an elongation at break of 12% is shown in Fig. 7 (right). For the latter, necking can be observed in the specimen failure area, which matches the characteristic stress–strain curve of the tensile test (see Fig. 4). The same applies to the specimen loaded in the creep test, where the neck of the specimen is as well evident in the creep curve (see Fig. 6). What is particularly remarkable is that there are also shear bands clearly visible in the necked epoxy specimen region of the tensile and creep loaded and thereby plastically deformed specimens, which is very unusual for thermoset materials in general and for epoxy resins in particular.

Regions of plastic deformation due to shear stress are actually a typical example of the non-linear deformation behavior of thermoplastics, e.g. acrylonitrile-butadiene-styrene copolymerisate (ABS). The shear bands represent an inhomogeneity of orientation and usually occur at an angle of ±45° to 55° to the direction of loading (this angle may deviate due to superposition with normal stresses which leads to a maximum of shear stresses in 45° to 55° direction to the load) [46]. The formation of shear bands is favored by a stress-related decrease in volume [47]. However, the explanations for thermoplastics cannot be directly transferred to thermosets, since they are closely cross-linked and slippage of macromolecular chains should not be possible.

Digital image correlation (DIC) is a method to visualize the local strain (and therefore also stress) over the whole sample area during a tension test. This is shown in Fig. 8 for a 100 µm thick and plastically deformed sample at a relatively high stress and a total strain of 20% close to the value of elongation at break for this sample. It is clearly visible that regions with relatively high local strains (over 40%) shear bands develop.

In order to gain a deeper understanding of the molecular mechanisms that cause this mechanical behavior, infrared spectroscopy (IR) is applied. In the following section, the results of the IR analysis are presented.

3.4. Infrared spectroscopy

Due to the *ex situ* and *in situ* IR analysis, load induced spectral changes can be detected. A theoretical explanation for these so-called peak shifts can give the Badger's rule (Eq. (1)) and the relationship between the peak wavenumber and the bond stiffness k of the corresponding vibrational bonds (Eq. (2)). The Badger rule asserts that the bond stiffness k_{ij} of a diatomic molecule ij is anitproportional to the bond length l_{ij} between two atoms i and j [48,49]. The two parameters involved c_{ij} and d_{ij} are atom-specific constants. If the bond length l_{ij} in a molecule or between two atoms i and j increases due to a load introduction, the bond stiffness k_{ij} decreases and as a consequence the corresponding vibrational peak wavenumber $\tilde{\upsilon}_{ij}$ shifted towards lower values, which can be detected in the IR spectrum.

$$c_{ij} = \mathbf{k_{ij}} \cdot (l_{ij} - d_{ij})^p \tag{1}$$

$$\tilde{\upsilon}_{ij} = \frac{1}{2\pi} \cdot \sqrt{\frac{\mathbf{k_{ij}}}{\mu_{ij}}} \tag{2}$$

The first necessary requirement for *ex situ* and *in situ* IR measurement on loaded epoxy films is that vibrational modes of stress-sensitive bonds are found in the spectrum. Moreover, extracting peak shifts and spectral changes from complex spectra with overlapping, mutually and dependently shifting peaks is challenging as well. It is often only possible to consider well-resolved bands of relatively high intensity [50]. Therefore, total absorbance or relatively less intensity of the stress-sensitive bonds are not appropriate for the developed method. The vibration modes of the stress-sensitive bonds usually consist of at least one molecular component that is involved in a load-bearing action in the skeleton of the chain [51]. As observed in the study of Doblies et al. on epoxy samples, some peaks of stress-sensitive bonds show a load-induced change in the associated peak wavenumber [52]. Thus, a wavenumber-dependent change under loading can also be detected in cross-linked epoxy. This allows an evaluation of the correlation

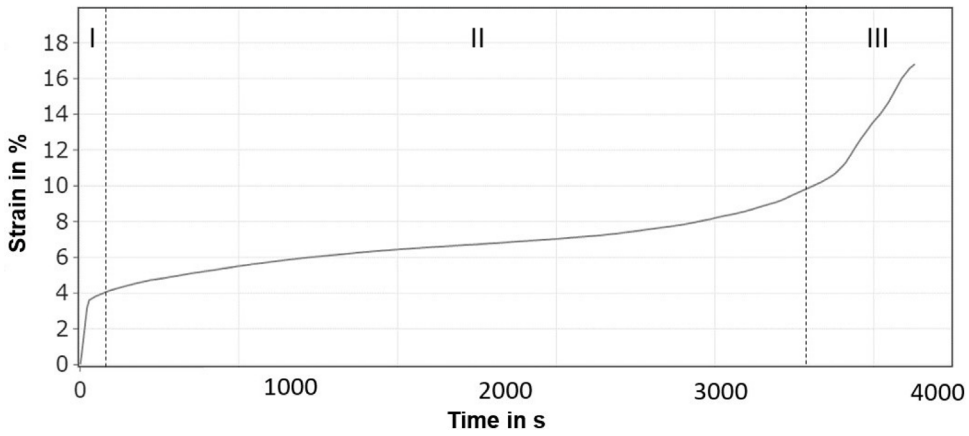

Fig. 6. Creep curve of a representative film specimen with a thickness of 30 μm (Deben tensile microstage). The creep graph shows the strain evolution over time for 56 MPa (80% UTS) and the three creep phases.

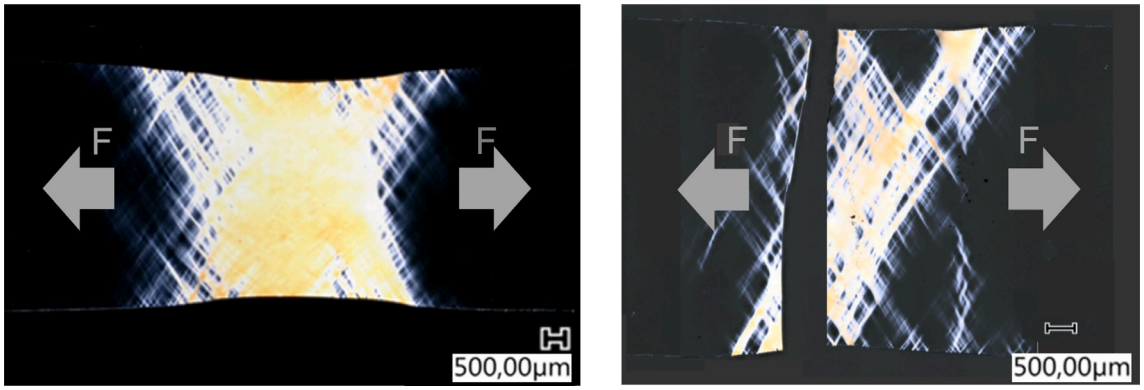

Fig. 7. Representative birefringence images of a film specimen (30 μm) at an elongation of 16% during creep test (left) and a film specimen (30 μm) after tensile test with failure (right), both illustrating necking and shear bands in 45° to 55° direction to load.

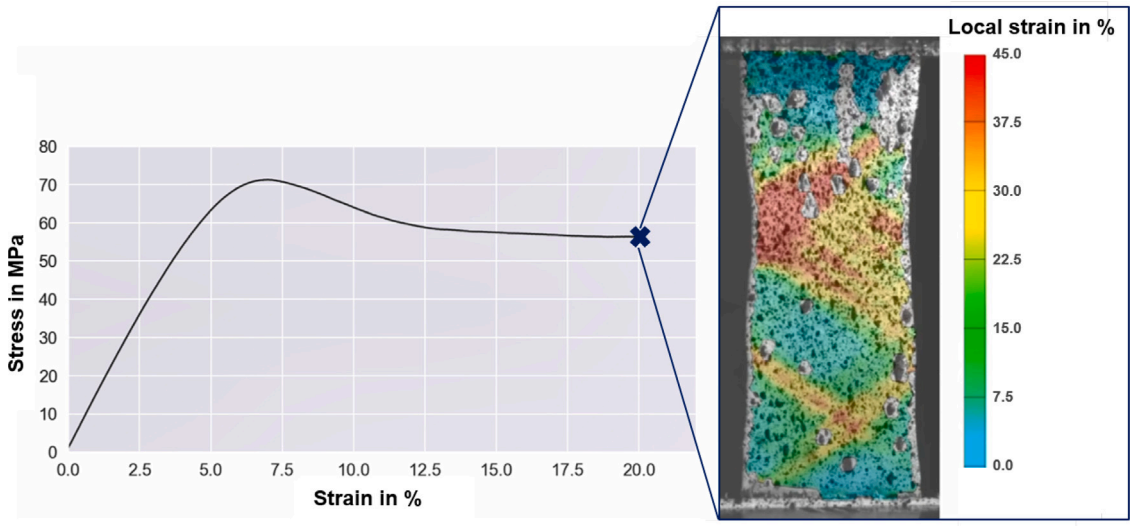

Fig. 8. Stress–strain curve of a film specimen (thickness of 100 μm) recorded during a tension test at room temperature with a strain rate 1 mm/min. Additionally the DIC image for the total strain of 20% is shown with the visualized local strain values. It is clearly visible that high local elongation (over 40%) occurs in areas of the shear bands or in their direction.

between peak position or wavenumber and stress-sensitive molecular components in epoxy and their structural changes. However, the ether peaks (first overtone at 2070 cm^{-1}) selected in the study of epoxy by Doblies et al. were not found to be a suitable vibration mode for the present study due to the low intensity caused by the comparatively lower sample thickness (Lambert–Beer's law) [53]. However, in this study, the peak of the intramolecular aromatic C–C bonds exhibits load-induced wavenumber changes toward lower values. More in detail, the corresponding peak $\tilde{\upsilon}_{aro}$ at 1608 cm^{-1} is accompanied by a stretching of the aromatic ring. The peak can be found in the measured IR spectrum

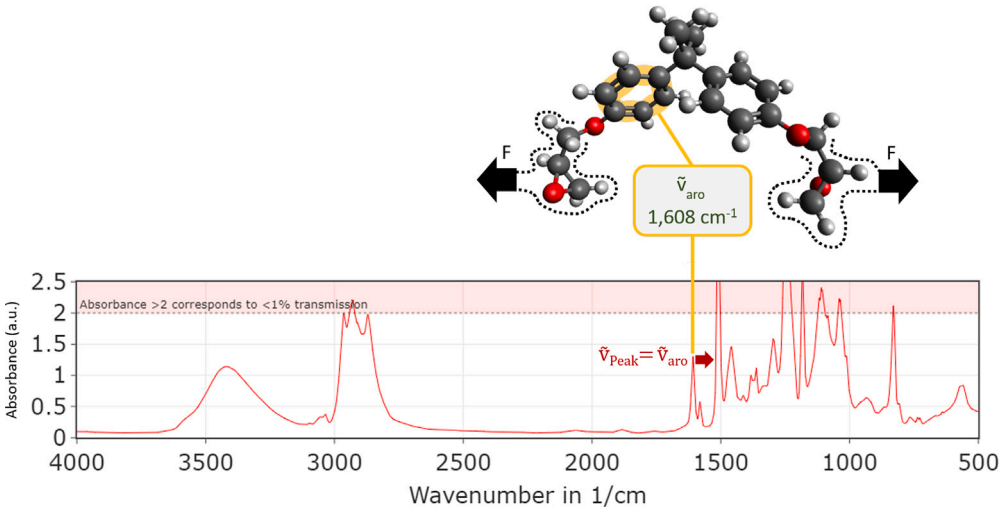

Fig. 9. Molecular backbone structure of epoxy films including the aromatic para-phenylene group, which is also marked in a representative IR spectrum of an unloaded epoxy film specimen. All peaks in the red colored absorbance region are not suitable for the in situ tracking of the peak positions due to the high or total absorbance.

of an unloaded epoxy film specimen schematically illustrated in Fig. 9. Since the aromatic molecules or more precisely the para-phenylene group and the corresponding (carbon) bonds are part of the backbone, they are directly responsible for the force transmission during the load application to the film sample through covalent bonds.

Due to comparatively small changes in peak position or peak wavenumber, a thorough evaluation of the spectral IR raw data is required for an identification. Analogously to the study of Doblies et al. [52], a so-called peak fitting is performed by approximating a model function to stress-sensitive peaks from the measured raw IR data. Solids can be approximated in this way with Gaussian distribution [53] and the characteristic features of the distribution can be extracted. The Gaussian model is defined as a function of area, mean and standard deviation and is fitted to the measured data using PythonLibrary lmfit to approximate the measured data. The approximation is based on the method of the smallest squares and minimizes thereby the sum of the error squares between the model function and the measured data. Fig. 10 shows the procedures performed, from raw data through the optimized model function to the determination of the parameters of interest for the investigation or the so-called feature extraction. At the beginning of the evaluation, a baseline correction and normalization is performed. Normalization serves mainly to compensate thickness differences of the films and the changes in the thickness of the film caused by the load introduced necking. For this purpose, a Min-Max normalization is used, which scales all absorbance values of the recorded IR data to a range between 0 and 1. As a further step of the data preprocessing, an interpolation of the measured IR data is carried out. With the selected settings for the IR spectrometer (Bruker, Tensor II, see 2.4.1) two measured wavenumbers within a spectrum have a distance of approximately $\Delta\tilde{\nu}_{aro} = 0.7\,cm^{-1}$. A third-degree spline interpolation is used to compact the data and reduce the distance to $0.001\,cm^{-1}$. When the compacted data set is deriving, a more accurate determination of the inflection points is possible. The inflection points are then used as limits of the data range, which serve for the approximation of the model function. Afterwards, the model function is approximated between the inflection points. Finally, the interesting parameters can be determined. In the following, the focus is on load-induced peak shifts in ductile epoxy films, i.e. changes of the aromatic peak wavenumber $\tilde{\nu}_{aro}$ of 1608 cm^{-1}. For this purpose, the approximated model function is derived and in this way the wavenumber belonging to the maximum of the selected peak is determined. This can be done for all measured IR spectra, recorded *ex situ* before and after mechanical loading (see 2.4.1) and *in situ* during creep tests on epoxy films (see 2.4.2). Both methods allow tracking of the peak position or wavenumber of stress-sensitive bonds, such as for the aromatic para-phenylene group. This allows the determination of the peak shift $\Delta\tilde{\nu}_{aro}$ representing changes in the molecular structure of the backbone (see Fig. 9) induced by the introduction of mechanical load.

3.4.1. *Ex situ infrared spectroscopy at room temperature*

The changes in the molecular backbone induced by load are analyzed by comparing the IR spectrum of the as-produced or unloaded film samples and at room temperature tensile loaded film samples with a thickness of 30 µm. For this purpose, 100 IR spectra in an investigated circular area with a diameter of 4 mm per specimen position are recorded. According to the IR evaluation steps of the raw IR data (see Fig. 10), all recorded spectra are preprocessed prior to comparison. Due to small load-induced changes of a peak wavenumber, the scattering was investigated. The scattering of peak wavenumber $\tilde{\nu}_{aro}$ is 1608 ± $0.02\,cm^{-1}$, which is significantly lower than the amount of the measured peak shifts, so that it cannot be explained by scattering.

Therefore, a difference in the peak of the aromatic para-phenylene group with respect to the associated peak position or wavenumber $\tilde{\nu}_{aro}$ at 1608 cm^{-1} can be identified. After mechanical loading, plastically deformed samples showed that the center of the aromatic peak or the maximum $\tilde{\nu}_{aro}$ is shifted to lower wavenumbers compared to as-produced films. This allows the conclusion that the molecular structure in epoxy has changed under mechanical load. To observe this in more detail, in total, three different IR measurements per film specimen are performed (1. As-produced specimen before mechanical loading, 2. Sample area of plastic deformation with shear bands and necking after loading and 3. Sample region without visually visible plastic deformation after loading), as shown in Fig. 11.

The sample region with shear bands (2.) exhibits a significantly lower wavenumber for the aromatic C–C peak even after stress relief due to final failure, while the peak wavenumber $\tilde{\nu}_{aro}$ for sample regions without visible plastic deformation (3.) shows a higher wavenumber value in comparison. The latter is close to the value of the initial condition of the as-produced film specimen without loading (1.). Plastic deformation or shear bands result in a permanent and non-reversible molecular change of the aromatic C–C bonds or other bonds associated with this molecular vibration mode due to the introduction of mechanical stress. However, from a chemical point of view, this cannot be the comprehensive explanation. The para-phenylene group is a very rigid and highly sterically hindered molecule with high bond strength and stiffness k_{aro} compared to other molecular components of the epoxy backbone. This means that a relatively high amount of energy

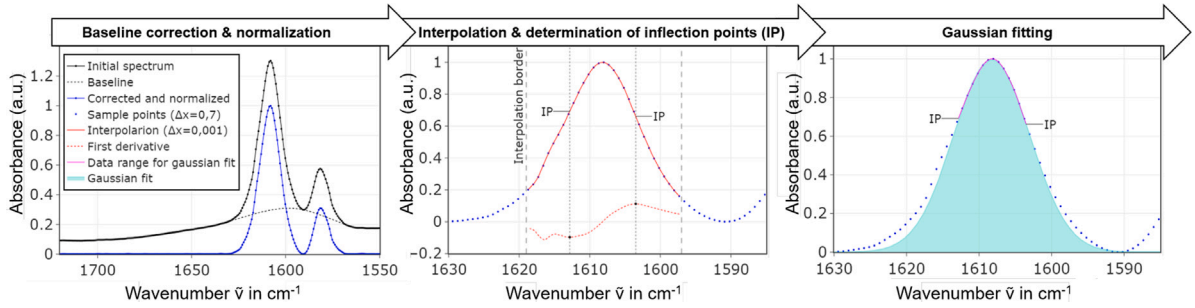

Fig. 10. Schematic evaluation steps of the raw IR data via python ($\Delta x = \Delta\tilde{\nu}_{aro}$).

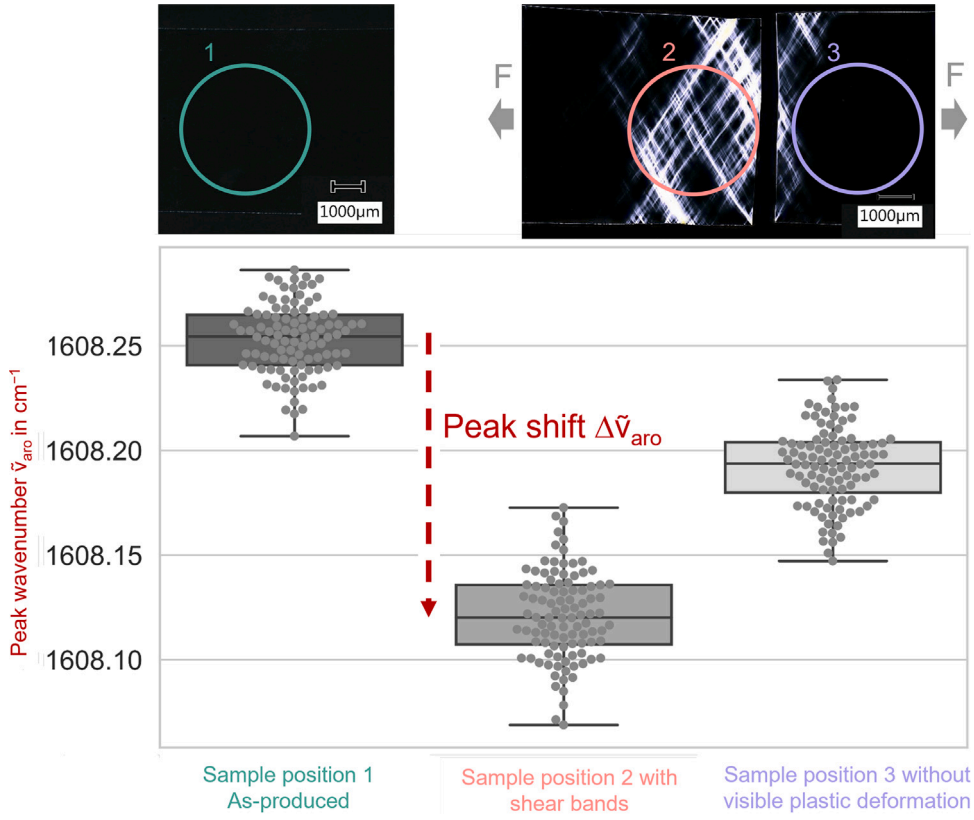

Fig. 11. Wavenumbers of the aromatic peak $\tilde{\nu}_{aro}$ for an unloaded film sample with a thickness of 30 µm and different specimen regions of the film specimen after tensile test at room temperature and the birefringence image corresponding to the loaded and failed film sample.

is required to cause length changes of the aromatic C–C bonds. At such high energies, numerous bond dissociations of other, weaker molecular backbone bonds would occur. This would also have to be detected in the IR spectrum by a decrease in the intensity of the corresponding peaks. However, no further or evaluable spectral changes could be detected for other peaks in the IR spectrum of the epoxy films during mechanical loading although the changes of the aromatic C–C bonds could be clearly demonstrated. To get more information about the load-induced molecular mechanisms, the test temperature influence on the mechanical behavior and the aromatic peak shift is investigated.

3.4.2. *Ex situ infrared spectroscopy at different temperatures*

To investigate the possible influence of temperature on these changes in the aromatic structure under load introduction, the preprocessed position of the aromatic peak $\tilde{\nu}_{aro}$ before and after mechanical loading is determined at different test temperatures. Using this method, the difference between peak wavenumber before and after load $\Delta\tilde{\nu}_{aro}$ can be correlated with the mechanical stress–strain curve of films with a thickness of 50 µm or, more precisely, with the non-uniform plastic deformation energy. For this purpose, the area under the stress–strain curves of the tensile tests (see Fig. 5) is determined, which serves as a measure of the energy which is associated with the deformation process. The area under the curve can be divided into an elastic energy (E_{el}) and a plastic energy (E_{pl}) deformation region. After elastic deformation, plastic deformation occurs throughout the whole sample ($E_{pl,uniform}$), while after the necking is formed, the plastic deformation occurs more in the region of necking ($E_{pl,non\text{-}uniform}$). This assignment of the sub-areas can be seen in Fig. 12 (left).

As already seen in Fig. 5, the film samples reaches higher elongation and plastic deformation at higher temperatures. Therefore more $E_{pl,non\text{-}uniform}$ is converted at higher temperatures, even if the strength is reduced. Fig. 12 (right) shows the ratio of the measured peak shift to the energy $E_{pl,non\text{-}uniform}$ introduced for the different test temperatures. Despite the relatively small number of investigated samples, the trend shows that the ratio of peak shift $\Delta\tilde{\nu}_{aro}$ (here before loading vs. after loading) to non-uniform plastic energy $E_{pl,non\text{-}uniform}$ increases linearly with temperature. This means that at a higher temperature, for the same amount of non-uniform plastic energy $E_{pl,non\text{-}uniform}$ introduced

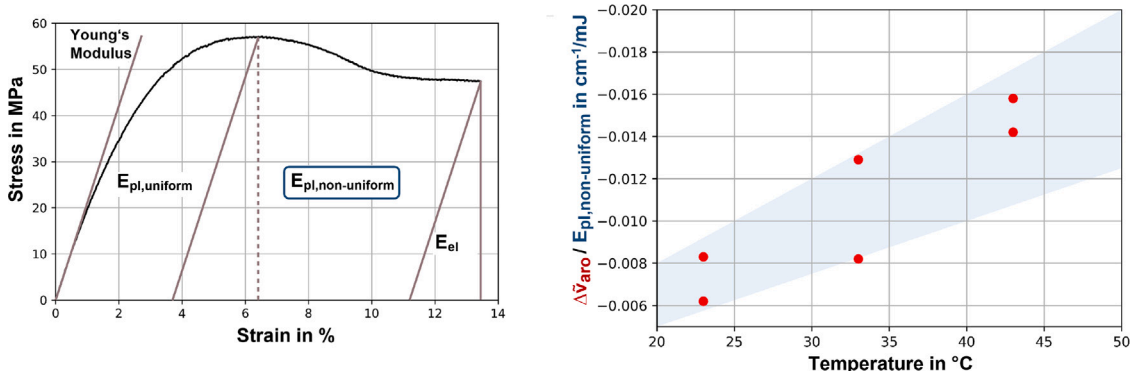

Fig. 12. Schematic representation of a stress–strain curve including indication of the energy types for the respective section (left) and the aromatic peak shift or wavenumber $\Delta\tilde{\upsilon}_{aro}$ (before loading vs. after loading) related to the plastic non-uniform $E_{pl,non\text{-}uniform}$ deformation energy as a function of the tensile test temperature (right).

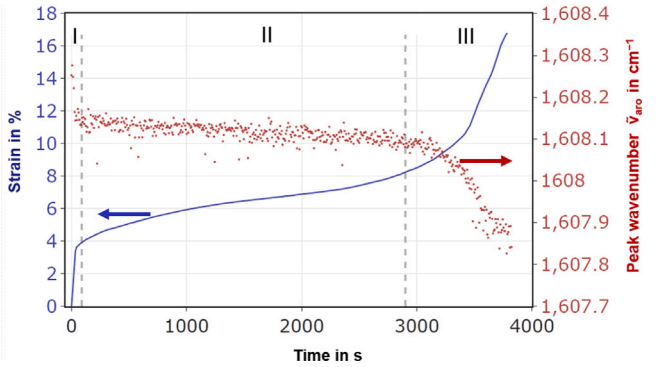

Fig. 13. Aromatic peak wavenumber $\tilde{\upsilon}_{aro}$ around 1608 cm^{-1} for a representative film specimen with a thickness of 30 µm over the time during the creep loading (red curve) and the corresponding creep curve of the microstage at room temperature with a load of 56 MPa (blue curve).

into the necking, the peak shift $\tilde{\upsilon}_{aro}$ increases more. Therefore, a significant impact of the test temperature during mechanical loading on the molecular mechanisms that occur during plastic deformation of the epoxy can be detected.

3.4.3. *In situ infrared spectroscopy at room temperature*

To analyze the molecular mechanisms of the para-phenylene group $\tilde{\upsilon}_{aro}$ at 1608 cm^{-1} during mechanical loading, the peak wavenumber is tracked and preprocessed (see Fig. 10) during a creep experiment, i.e. *in situ*. When comparing a creep curve and the corresponding peak wavenumber $\tilde{\upsilon}_{aro}$ of a 30 µm thick representative film recorded during the mechanical creep load of 56 MPa in Fig. 13, it is noticeable that the course of the peak wavenumber $\tilde{\upsilon}_{aro}$ of the aromatic C–C stretching can be directly correlated with the mechanical deformation of the epoxy resin film.

Considering the relationships between molecular bond stiffness and lengths and the corresponding peak wavenumber (see Section 3.4), the aromatic peak shift $\Delta\tilde{\upsilon}_{aro}$ can be explained as follows: At the beginning of the creep test, there is a strong increase in sample strain and also an increase in the C–C bond length l_{CC} relected in the decrease of bond stiffness k_{CC} and thus in the peak wavenumber $\tilde{\upsilon}_{CC}$ or more general $\tilde{\upsilon}_{aro}$ (Eq. (2), constant reduced diatomic molecule mass μ_{ij} or μ_{CC}). As the experiment progresses, the peak position or wavenumber of the aromatic para-phenylene groups $\tilde{\upsilon}_{aro}$ is relatively constant as the sample strain (creep phase 2). A further decrease of $\tilde{\upsilon}_{aro}$ towards the end of the creep test corresponds to the strain-induced necking of the sample (creep phase 3). Thus, it can be seen that a shift of the aromatic C–C stretching peak to lower wavenumbers occurs with increasing creep duration in the polymer network, indicating an extension of the C–C bond length l_{CC} and confirming previous studies with other backbone bonds [18,20,52]. Due to the already mentioned high bond stiffness and strength of the C–C bonds in the para-phenylene group, this cannot be the whole explanation for the load-induced molecular mechanisms and the determined aromatic peak shift resulting from the plastic deformation process. Verschatse et al. explain the high plastic deformation of microfibers made from the same epoxy resin system with a rearrangement of the epoxy network structure due slippage of the chains in the internal network [1,43,54,55] and draw a kind of analogy to the plastic deformation behavior of thermoplastics [56]. Concerning this, the aromatic peak shift may be due to the reorientation of the para-phenylene group in the backbone under load or in the shear bands resulting in a changed chemical environment. If so, other bonds involved in the aromatic vibration, such as the hydrogen atoms bonded on the aromatic para-phenylene group, can influence the changes in the aromatic wavenumber as well. Another hypothesis is, that under load, recombination of bonds is energetically more favorable than dissociation. This was observed in the study of Konred et al. from molecular dynamics simulation [57]. The hypothetical approaches will be investigated more in detail in further studies. However, in this study, it has been proven that the backbone or the aromatic para-phenylene groups in the epoxy films are stress sensitive and respond to mechanical loading with changes in molecular structure that cause an IR peak shift at 1608 cm^{-1}. This phenomenon has also been observed in other, molecular non-isotropic structured, materials such as high modulus polymer fibers like PBO and aromatic polyamide, where a load-induced peak shift of the aromatic stretching at 1610 cm^{-1} could be detected in Raman spectra [27].

4. Summary and outlook

We introduce a new manufacturing technique to produce epoxy films with a thickness between 15 and 100 µm, which are in the size range or dimension of resin-rich zones between fibers (1–25 µm, intralayer) and resin-rich zones between reinforcing prepregs or layers (10–200 µm, interlayer) in polymeric composites [1]. The glass transition temperature T_g of the epoxy films is determined by DSC and is within the range of the data sheet and standard bulk samples nearly independent from the specimen size (bulk vs. film).

During tensile and creep tests, these films show atypical plasticity with shear band formation and necking. The shear bands can be visualized via photoelasticity and correlated with the sample regions of maximum local deformation or elongation of more than 40% as well as with a change in molecular structures, visible via changes of wavenumber in IR spectra. Plasticity and necking behavior are also evident in the tensile and creep curves for all film specimen thicknesses. The origin of plasticity has been found to be connected to the gauge volume, as known from the literature [1,43,44,58,59]. A reduction in the gauge volume from a standard bulk to thin films thus leads to

different molecular mechanisms occurring in tensile loaded films and results in a higher plasticity. It might be that the molecular mobility is increased and the molecular interactions between the elements are reduced by a decrease in the gauge volume, resulting in a higher cooperative mobility of the entire system. The result is an increase in plasticity, which in bulk samples occurs only at elevated temperatures close to T_g.

To explain the formation of shear bands on a microscopic level, the mechanisms that occur on a molecular level must be further investigated. In the future, an infrared microscope with very high spatial resolution will be used for this purpose. Moreover, a Raman microscope will be used to also analyze the IR inactive bonds and peaks.

Additionally, further resin systems and further bonds or vibrational modes will be analyzed. Wide-angle X-ray scattering (WAXS) investigations based on the study of epoxy fibers by Sui et al. [43] can also be carried out to further investigate molecular alignment in epoxy films. By applying polarized IR radiation, shear band regions in plastically deformed epoxy films can also be examined with regard to potential molecular orientations to further explain the shear band formation and the causing molecular mechanisms.

To understand the molecular processes, their interactions, and their reasons more precisely on the basis of the experiments carried out, a molecular simulation approach will be a valuable and powerful tool [57]. The knowledge gained with the results from this study and further experiments and simulation can be used for the targeted development and further structural optimization of polymer composites and their manufacturing.

CRediT authorship contribution statement

Janina Mittelhaus: Conceptualization, Methodology, Formal analysis, Investigation, Writing – original draft, Visualization. **Phil Röttger:** Formal analysis, Investigation. **Eduard Schill:** Formal analysis, Investigation. **Julius Jacobs:** Formal analysis, Investigation. **Bodo Fiedler:** Conceptualization, Methodology, Writing – review & editing, Supervision, Project administration, Funding acquisition.

Declaration of competing interest

The authors declare that they have no known competing financial interests or personal relationships that could have appeared to influence the work reported in this paper.

Data availability

Data will be made available on request.

Acknowledgments

This research is part of the project “Mechanisms of thermoset plasticity explained on the basis of spectroscopic analysis and atomistic simulations” with the project number 525597740 funded by German Research Foundation (DFG). This financial support is gratefully acknowledged. Publishing fees supported by Funding Programme Open Access Publishing of Hamburg University of Technology (TUHH).

References

[1] O. Verschatse, L. Daelemans, W.V. Paepegem, K. de Clerck, In-situ observations of microscale ductility in a quasi-brittle bulk scale epoxy, Polymers 12 (11) (2020) http://dx.doi.org/10.3390/polym12112581.
[2] A. D638-22, Standard test method for tensile properties of plastics, Book Stand. Vol. 08.01 (2022) http://dx.doi.org/10.1520/D0638-22.
[3] DIN EN ISO 527-1, Bestimmung der zugeigenschaften – teil 1: Allgemeine grundsätze, 2019, http://dx.doi.org/10.31030/3059426.
[4] F.A. Gilabert, D. Garoz, R. Sevenois, S. Spronk, A. Rezaei, W.V. Paepegem, ESCM, Composite micro-scale model accounting for debonding, strain-rate dependence and damage under impact using an explicit finite element solver, 17th Eur. Conf. Compos. Mater. (2016) 1–8.
[5] T.J. Vaughan, C.T. McCarthy, Micromechanical modelling of the transverse damage behaviour in fibre reinforced composites, Compos. Sci. Technol. 71 (3) (2011) 388–396, http://dx.doi.org/10.1016/j.compscitech.2010.12.006.
[6] W. Tan, F. Naya, L. Yang, T. Chang, B.G. Falzon, L. Zhan, J.M. Molina-Aldareguía, C. González, J. LLorca, The role of interfacial properties on the intralaminar and interlaminar damage behaviour of unidirectional composite laminates: Experimental characterization and multiscale modelling, Composites B 138 (2018) 206–221, http://dx.doi.org/10.1016/j.compositesb.2017.11.043.
[7] M.-F. Ren, X.-W. Zhang, C. Huang, B. Wang, T. Li, An integrated macro/micro-scale approach for in situ evaluation of matrix cracking in the polymer matrix of cryogenic composite tanks, Compos. Struct. 216 (2019) 201–212, http://dx.doi.org/10.1016/j.compstruct.2019.02.079.
[8] C. González, J. LLorca, Multiscale modeling of fracture in fiber-reinforced composites, Acta Mater. 54 (16) (2006) 4171–4181, http://dx.doi.org/10.1016/j.actamat.2006.05.007.
[9] J. LLorca, C. González, J.M. Molina-Aldareguía, J. Segurado, R. Seltzer, F. Sket, M. Rodríguez, S. Sádaba, R. Muñoz, L.P. Canal, Multiscale modeling of composite materials: a roadmap towards virtual testing, Adv. Mater. 23 (44) (2011) 5130–5147, http://dx.doi.org/10.1002/adma.201101683.
[10] L. Mishnaevsky, Composite materials for wind energy applications: micromechanical modeling and future directions, Comput. Mech. 50 (2) (2012) 195–207, http://dx.doi.org/10.1007/s00466-012-0727-5.
[11] E. Totry, J.M. Molina-Aldareguía, C. González, J. LLorca, Effect of fiber, matrix and interface properties on the in-plane shear deformation of carbon-fiber reinforced composites, Compos. Sci. Technol. 70 (6) (2010) 970–980, http://dx.doi.org/10.1016/j.compscitech.2010.02.014.
[12] A.J. Kinloch, D.G. Gilbert, S.J. Shaw, A mechanism for ductile crack growth in epoxy polymers, J. Mater. Sci. 21 (1986) 1051–1056, http://dx.doi.org/10.1007/BF01117394.
[13] R.P. Wool, Mechanisms of frequency shifting in the infrared spectrum of stressed polymers, J. Polym. Sci. B 13 (1975) 1795–1808, http://dx.doi.org/10.1002/pol.1975.180130912.
[14] A. Sturcová, S.J. Eichhorn, M.C. Jarvis, Vibrational spectroscopy of biopolymers under mechanical stress: processing cellulose spectra using bandshift difference integrals, Biomacromolecules 7 (9) (2006) 2688–2691, http://dx.doi.org/10.1021/bm060457m.
[15] S.N. Zhurkov, V.E. Korsukov, I.I. Novak, V.I. Vettegren, Determination of overstressed chemical bonds in polymers by the method of infrared spectroscopy, Fiz. Tverd. Tela 11 (2) (1969) 290–295.
[16] V.I. Vettegren, I.I. Novak, Determination of atomic stress distribution in stressed polymers by infrared spectroscopy, J. Polym. Sci. B 11 (1973) 2135–2142, http://dx.doi.org/10.1002/pol.1973.180111105.
[17] V.I. Vettegren, I.I. Novak, Determination of the true stresses on interatomic bonds in loaded polymers by the infrared spectroscopy method, Fiz. Tverd. Tela 15 (5) (1973) 1417–1422.
[18] V.I. Vettegren, I.I. Novak, K.J. Friedland, Overstressed interatomic bonds in stressed polymers, Int. J. Fract. 11 (5) (1975) 789–801, http://dx.doi.org/10.1007/BF00012897.
[19] V.M. Voroboyev, I.V. Razumovskaya, V.I. Vettegren, Deformation of interatomic bonds in polymers, Polymer 19 (11) (1978) 1267–1272, http://dx.doi.org/10.1016/0032-3861(78)90303-8.
[20] D.K. Roylance, K.L. DeVries, Determination of atomic stress distribution in oriented polypropylene by infrared spectroscopy, Polym. Lett. 9 (6) (1971) 443, http://dx.doi.org/10.1002/pol.1971.110090607.
[21] V.I. Vettegren, V.B. Kulik, Quantum vibration dynamics and deformation of skeleton of polymer molecules, Polym. Sci. Ser. A 51 (8) (2009) 849–857, http://dx.doi.org/10.1134/S0965545X0908001X.
[22] S.J. Eichhorn, R.J. Young, Deformation micromechanics of natural cellulose fibre network and composites, Compos. Sci. Technol. 63 (9) (2003) 1225–1240, http://dx.doi.org/10.1016/S0266-3538(03)00091-5.
[23] C. Galiotis, R.J. Young, P.H.J. Yeung, D.N. Batchelder, The study of model polydiacetylene/epoxy composites, part 1 the axial strain in the fibre, J. Mater. Sci. 19 (11) (1984) 3640–3648, http://dx.doi.org/10.1007/BF02396936.
[24] I.M. Robinson, R.J. Young, C. Galiotis, D.N. Batchelder, Study of model polydiacetylene/epoxy composites, part 2 effect of resin shrinkage, J. Mater. Sci. 22 (10) (1987) 3642–3646, http://dx.doi.org/10.1007/BF01161472.
[25] R.J. Young, R.J. Day, M. Zakikhani, I.M. Robinson, Fibre deformation and residual thermal stresses in carbon fibre reinforced PEEK, Compos. Sci. Technol. 34 (3) (1989) 243–258, http://dx.doi.org/10.1016/0266-3538(89)90031-6.
[26] C. Galiotis, N. Melanitis, D.N. Batchelder, I.M. Robinson, J.A. Peacock, Residual strain mapping in carbon fibre/PEEK composites, Composites 19 (4) (1988) 321–324, http://dx.doi.org/10.1016/0010-4361(88)90009-2.
[27] W.-Y. Yeh, R.J. Young, Molecular deformation processes in aromatic high modulus polymer fibres, Polymer 40 (4) (1999) 857–870, http://dx.doi.org/10.1016/S0032-3861(98)00308-5.
[28] R.J. Young, R.J. Day, M. Zakikhami, The structure and deformation behaviour of poly(p-phenylene benzobisoxazole) fibres, J. Mater. Sci. 25 (1990) 127–136, http://dx.doi.org/10.1007/BF00544197.
[29] W.-Y. Yeh, R.J. Young, Deformation processes in poly(ethylene terephthalate) fibers, J. Macromol. Sci. B 37 (1) (1998) 83–118, http://dx.doi.org/10.1080/00222349808220457.

[30] C. Galiotis, I.M. Robinson, R.J. Young, B.J.E. Smith, D.N. Batchelder, Strain dependence of the Raman frequencies of a kevlar 49 fibre, Polym. Commun. 26 (12) (1985) 354–355.
[31] S. van der Zwaag, M.G. Northolt, R.J. Young, I.M. Robinson, C. Galiotis, D.N. Batchelder, Chain stretching in aramid fibers, Polym. Commun. 28 (1987) 276–277.
[32] I.M. Robinson, M. Zakikhani, R.J. Day, R.J. Young, C. Galiotis, Strain dependence of the Raman frequencies for different types of carbon fibres, J. Mater. Sci. Lett. 6 (10) (1987) 1212–1214, http://dx.doi.org/10.1007/BF01729187.
[33] C. Galiotis, D.N. Batchelder, Strain dependences of the first- and second-order Raman spectra of carbon fibres, J. Mater. Sci. Lett. 7 (5) (1988) 545–547, http://dx.doi.org/10.1007/BF01730722.
[34] S.J. Eichhorn, Sirichaisit, R.J. Young, Deformation mechanisms in cellulose fibres, paper and wood, J. Mater. Sci. (36) (2001) 3129–3135, http://dx.doi.org/10.1023/A:1017969916020.
[35] S.J. Eichhorn, R.J. Young, W.-Y. Yeh, Deformation processes in regenerated cellulose fibers, Text. Res. J. 71 (2) (2001) 121–129, http://dx.doi.org/10.1177/004051750107100206.
[36] A. Sturcová, G.R. Davies, S.J. Eichhorn, Elastic modulus and stress-transfer properties of tunicate cellulose whiskers, Biomacromolecules 6 (2) (2005) 1055–1061, http://dx.doi.org/10.1021/bm049291k.
[37] B. Hinterstoisser, M. Akerholm, L. Salmén, Load distribution in native cellulose, Biomacromolecules 4 (5) (2003) 1232–1237, http://dx.doi.org/10.1021/bm030017k.
[38] P. Peetla, K.C. Schenzel, W. Diepenbrock, Determination of mechanical strength properties of hemp fibers using near-infrared fourier transform Raman microspectroscopy, Appl. Spectrosc. 60 (6) (2006) 682–691, http://dx.doi.org/10.1366/000370206777670602.
[39] J. Sirichaisit, V.L. Brookes, R.J. Young, F. Vollrath, Analyis of structure/property relationships in silkworm (bombyx mori) and spider dragline (nephila edulis) silks using raman spectroscopy, Biomacromolecules 4 (2) (2003) 387–394, http://dx.doi.org/10.1021/bm0256956.
[40] J. Sirichaisit, R.J. Young, F. Vollrath, Molecular deformation in spider dragline silk subjected to stress, Polymer 41 (2000) 1223–1227, http://dx.doi.org/10.1016/S0032-3861(99)00293-1.
[41] DIN EN ISO 11357-2, Kunststoffe - dynamische differenzkalorimetrie DSC - teil 2: Bestimmung der glasübergangstemperatur und der glasübergangsstufenhöhe, 2020, http://dx.doi.org/10.31030/3127571.
[42] D. Bryce, J. Thomason, L. Yang, Micromechanical and spectroscopic characterisation of the curing performance of epoxy resins in the microbond test: 41st risøinternational symposium on materials science, IOP Conf. Ser.: Mater. Sci. Eng. (942) (2020) http://dx.doi.org/10.1088/1757-899X/942/1/012019.
[43] X.M. Sui, M. Tiwari, I. Greenfeld, R.L. Khalfin, H. Meeuw, B. Fiedler, H.D. Wagner, Extreme scale-dependent tensile properties of epoxy fibers, Express Polym. Lett. 13 (11) (2019) 993–1003, http://dx.doi.org/10.3144/expresspolymlett.2019.86.
[44] J. Misumi, R. Ganesh, S. Subramani Sockalingam, J. Gillespie. Jr., J. Misumi, R. Ganesh, S. Sockalingam, J.W. Gillespie, Experimental characterization of tensile properties of epoxy resin by using micro-fiber specimens, J. Reinf. Plast. Compos. 35 (24) (2016) 1792–1801, http://dx.doi.org/10.1177/073168441666924.
[45] J. Drummer, D. Gibhardt, J. Körbelin, B. Fiedler, General influence of the environmental temperature on the matrix strength under tensile and compressive loading - a comprehensive study on high performance matrices, Compos. Sci. Technol. 230 (Part 2) (2022) http://dx.doi.org/10.1016/j.compscitech.2022.109486.
[46] G.W. Ehrenstein, Polymer Werkstoffe: Struktur-Eigenschaften-Anwendung, third ed., Carl Hanser, München, 2011, http://dx.doi.org/10.3139/9783446429673.
[47] W. Retting, Mechanik der Kunststoffe: Die mechanischen Eigenschaften von Polymer-Werkstoffen, Carl Hanser, München, 1992.
[48] R.M. Badger, A relation between internuclear distances and bond force constants, J. Chem. Phys. 2 (3) (1934) 128–131, http://dx.doi.org/10.1063/1.1749433.
[49] R.S. Bhatta, P.P. Iyer, A. Dhinojwala, M. Tsige, A brief review of badger–bauer rule and its validation from a first-principles approach, Modern Phys. Lett. B 28 (29) (2014) http://dx.doi.org/10.1142/S0217984914300142.
[50] S.-I. Morita, Y. Ozaki, Pattern recognitions of band shifting, overlapping, and broadening using global phase description derived from generalized two-dimensional correlation spectroscopy, Appl. Spectrosc. 56 (4) (2002) 501–508, http://dx.doi.org/10.1366/00037020219549.
[51] R.P. Wool, Measurements of infrared frequency shifts in stressed polymers, J. Polym. Sci. B 19 (1981) 449–457, http://dx.doi.org/10.1002/pol.1981.180190305.
[52] A. Doblies, B. Fiedler, T. Würger, E. Schill, H.R. Meißner, C. Feiler, Mechanical degradation estimation of thermosets by peak shift assessment: General approach using infrared spectroscopy and atomistic simulations, Polymer 221 (2021) 123585, http://dx.doi.org/10.1016/j.polymer.2021.123585.
[53] P.R. Griffiths, J.A. Haseth, Fourier Transform Infrared Spectrometry, second ed., John Wiley & Sons, 2007, http://dx.doi.org/10.1002/047010631X.
[54] M. Harada, M. Morimoto, M. Ochi, Influence of network chain orientation on the mechanical property of epoxy resin filled with silica particles, J. Appl. Polym. Sci. 87 (Vol. 87 // 5) (2003) 787–794, http://dx.doi.org/10.1002/app.11454.
[55] A.T. Detwiler, A.J. Lesser, Aspects of network formation in glassy thermosets, J. Appl. Polym. Sci. 117 (2) (2010) 1021–1034, http://dx.doi.org/10.1002/app.31681.
[56] A.I. Leonov, A theory of necking in semi-crystalline polymers, Int. J. Solids Struct. 39 (24) (2002) 5913–5926, http://dx.doi.org/10.1016/S0020-7683(02)00478-X.
[57] J. Konrad, R.H. Meißner, E. Bitzek, D. Zahn, A molecular simulation approach to bond reorganization in epoxy resins: From curing to deformation and fracture, ACS Polym. Au (2021) http://dx.doi.org/10.1021/acspolymersau.1c00016.
[58] E.M. Odom, D.F. Adams, Specimen size effect during tensile testing of an unreinforced polymer, J. Mater. Sci. (27) (1992) 1767–1771, http://dx.doi.org/10.1007/BF01107202.
[59] T. Hobbiebrunken, B. Fiedler, M. Hojo, M. Tanaka, Experimental determination of the true epoxy resin strength using micro-scaled specimens, Composites A 38 (3) (2007) 814–818, http://dx.doi.org/10.1016/j.compositesa.2006.08.006.